Electron Injection, Recombination, and Halide Oxidation Dynamics at Dye-Sensitized Metal Oxide Interfaces

Todd A. Heimer and Edwin J. Heilweil*

National Institute of Standards and Technology, 100 Bureau Drive, Stop 8441, Gaithersburg, Maryland 20899

Carlo A. Bignozzi

Department of Chemistry, University of Ferrara, Via L. Borsari 46, 44100 Ferrara, Italy

Gerald J. Meyer

Department of Chemistry, Johns Hopkins University, 3400 North Charles Street, Baltimore, Maryland 21218

Received: September 27, 1999; In Final Form: November 17, 1999

Time-resolved infrared measurements indicate ultrafast, <350 fs, electron injection from $(4,4'dcb)_2Ru(NCS)_2$ (**1**) and $(5,5'dcb)_2Ru(NCS)_2$ (**2**) to nanostructured TiO_2 electrodes (where 4,4′dcb = $4,4'-(COOH)_2$-2,2′-bipyridine). Although rapid, the injection from **2** apparently occurs with a lower quantum yield than that from **1**, explaining a lower overall photon-to-current efficiency for **2**/TiO_2 solar cells. Transient visible spectroscopy reveals similar rates of both halide oxidation and injected electron-oxidized dye recombination for the two sensitizers. Substituting SnO_2 for TiO_2 increases the electron injection yield from **2** in the case of transparent metal oxide films and improves the photon-to-current efficiency. Results indicate a wavelength-dependent electron injection yield.

Introduction

Recent transient infrared measurements indicate that interfacial electron injection from the excited state of ruthenium polypyridyl sensitizers to TiO_2 electrodes occurs on the ultrafast (<1 ps) time scale.[1] This suggests electron injection can effectively compete with excited-state decay of the sensitizer; however, this does not always yield efficient photocurrent production.[2] A second competition exists between recombination of injected electrons with the oxidized Ru^{III} center and halide oxidation by Ru^{III}. This competition has been directly monitored in this work by measuring the rate of Ru^{II} recovery in the presence and absence of I^- using transient visible absorbance spectroscopy. Studies of two related sensitizers with significantly different excited-state reduction potentials and photovoltaic efficiencies, $(4,4'-(COOH)_2$-2,2′-bipyridine$)_2Ru(NCS)_2$ (**1**) and $(5,5'-(COOH)_2$-2,2′-bipyridine$)_2Ru(NCS)_2$ (**2**), suggest limitations and possible methods to improve the performance of dye-sensitized TiO_2 regenerative solar cells.

Photocurrent measurements for $(5,5'dcb)_2Ru(X)_2$ (where dcb = $(COOH)_2$-2,2′-bipyridine and X = NCS^-, CN^-, or Cl^-) on opaque TiO_2 nanostructured electrodes were part of a previous study.[3] These sensitizers were designed to enhance the spectral sensitivity of molecular solar cells toward longer wavelengths of light. Sensitizers utilizing the 5,5′dcb ligands have significantly lower excited-state reduction potentials compared to those of the corresponding 4,4′dcb analogues, which manifest in red-shifted absorbance spectra. This in turn improves the overlap of the absorbance spectra with the solar spectrum. The sensitizers in this series were compared with the 4,4′dcb analogues and in general displayed maximum incident photon-to-current conversion efficiencies (IPCEs) approximately one-half those of the 4,4′dcb sensitizers. Specifically, for **1** and **2** the maximum monochromatic IPCEs were 67.1 and 36.6%, respectively. It was concluded that the lower IPCE for **2** was due, at least in part, to a lower quantum yield for electron injection from the sensitizer excited state to the TiO_2 as nonradiative decay competes with electron injection.

Scheme 1 displays the relative energetics for **1** and **2** at the sensitizer−semiconductor interface.[4] Forward reactions which result in the production of photocurrent are electron injection (with rate constant k_2) and reduction of the oxidized sensitizer by a solution electron donor (k_4). Competing loss mechanisms include excited-state decay (k_1) and recombination of injected electrons with the oxidized sensitizer (k_3). The excited-state reduction potential of **2** (measured in solution) lies approximately 200 mV positive of that for **1**, resulting in a significant red shift in the absorbance spectrum. The conduction band of single-crystal SnO_2 lies approximately 300 mV lower in energy than that of TiO_2,[5] which may result in enhanced orbital overlap between the excited state of **2** and acceptors in the SnO_2.

Through the recent development of transparent TiO_2 films and use of time-resolved infrared (TRIR) spectroscopy, we are now able to quantify the electron-transfer rates at the semiconductor−sensitizer interface for **1** and **2** and make direct conclusions about the competitions between loss mechanisms and forward reactions. These results reinforce the findings of the previous work and also provide further insight into the fascinating nature of the sensitized metal oxide interface.

Experimental Section

Materials. Transparent TiO_2 films consisting of ≈16-nm-diameter TiO_2 particles were prepared by hydrolysis of Ti-(i-OPr)$_4$ as described previously in the literature.[6] Insulating ZrO_2 films were prepared from Zr(i-OPr)$_4$ in a similar fashion.[7] Transparent SnO_2 films were prepared using a slight modification of a published procedure:[8] One drop of Triton X-100

10.1021/jp993438y CCC: $19.00 © 2000 American Chemical Society
Published on Web 04/13/2000

SCHEME 1. Energy Levels at the Semiconductor−Sensitizer Interface

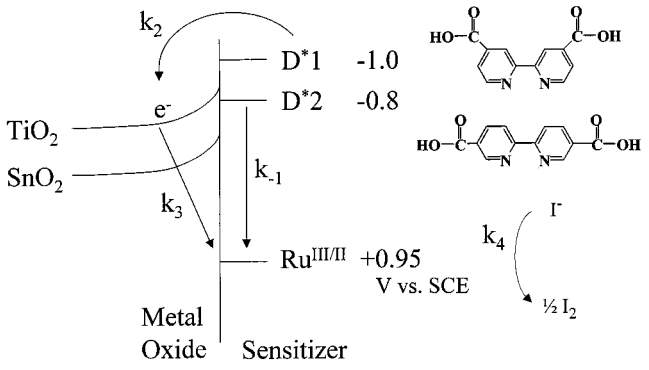

surfactant was added to 1 mL of 15% w/v SnO_2 colloidal aqueous solution (Alfa).[9] This mixture was deposited on the substrate and spread with a glass rod over an area masked with transparent tape. Two to five applications with 1-h room-temperature drying intervals were required to prepare SnO_2 films approaching 1 μm thick. Final sintering was performed at 400 °C for 1 h in air for all metal oxide films. Indium-doped tin oxide conductive glass substrates (Hartford Glass, 8 Ω) were used for transient visible experiments and photocurrent measurements. Unpolished CaF_2 substrates were used to prepare samples for mid-IR measurements.[10] Sensitizer **2** was available from previous studies.[3] Purified **1** was obtained from SolIdeas. Both sensitizers exhibited a single-exponential photoluminescence decay in MeOH upon laser excitation at 532 nm. Attachment of the sensitizers to the TiO_2 surface was achieved by soaking the TiO_2 films in MeOH solutions containing ≈5 mmol/L concentration of the sensitizer for 16 h.

Transient Spectroscopy. TRIR experiments were performed under the following conditions: The sample was excited at 20 Hz with 8 μJ of 590-nm, 150-fs fwhm synch-pumped dye laser output. The probe pulse consisted of a 250-fs broadband pulse spanning the range of 1850−1950 cm^{-1} generated by difference frequency mixing of two visible pulses in $LiIO_3$. The pump and probe beams were focused to approximately 200 μm diameter at the sample. Broadband detection of the probe was achieved directly using a 42 groove/mm single-grating spectrograph coupled to a 256 × 256 element MCT detector array. The pump−probe cross-correlation function, measured by a Si wafer, indicates an ≈350-fs instrument response function. Sample mounting was achieved by using the sensitized TiO_2 samples on CaF_2 as windows in a standard demountable IR cell. The cell was filled with dichloromethane such that the active area of the sample was bathed in the liquid. Samples of **2**/TiO_2 typically had an optical density at 590 nm, which was roughly half that of the **1**/TiO_2 samples. Therefore, TRIR experiments with **2**/TiO_2 were performed with both cell windows replaced by samples, such that approximately equal numbers of photons were absorbed in all cases. Further details of the TRIR apparatus can be found elsewhere.[11]

Transient visible absorbance experiments were performed using a Xe flashpack to produce white light broadband (350−900 nm) probe pulses of ≈3-μs duration. A Q-switched Nd:YAG laser was used to provide 5-ns fwhm excitation pulses at 532 nm, with energies of 0.05−0.25 mJ and a beam diameter of 2 mm. A double monochromator and photomultiplier tube were used for probe wavelength selection and detection. The system has a temporal instrument response of 14 ns.

An alternate apparatus was used in some cases to measure decay times on a shorter timescale. A Quantel Nd:YAG producing 30-ps fwhm, 532-nm pulses was used to excite the sample. A fraction of the 532-nm beam pumped a dye laser to provide 20-ps fwhm probe pulses. The dye laser was tuned to the wavelength of interest, typically 730 or 820 nm, and a monochromator/CCD was used for detection. The probe was delayed relative to the pump via an optical delay stage.

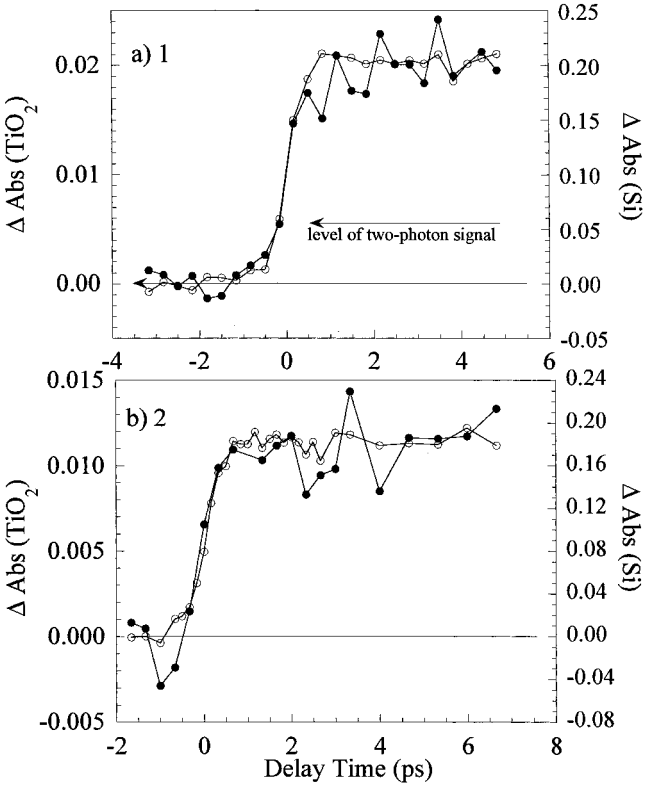

Figure 1. Rise time of the TiO_2 electron absorbance at 5.4 μm for (a) **1** and (b) **2** sensitized TiO_2 films in dichloromethane. Open circles indicate pump−probe cross-correlation measured in a Si wafer. Closed circles indicate absorbance by the injected electrons for sensitizers on TiO_2.

Photoelectrochemistry. Photocurrent measurements were performed by assembling the sensitized metal oxide electrode against a Pt-coated counter electrode, with a thin layer of 0.5 mol/L NaI and 0.05 mol/L I_2 electrolyte in propylene carbonate between the electrodes. A 150-W Xe lamp and single-grating monochromator served as the excitation source. Lamp output as a function of wavelength was measured with a NIST-calibrated Si photodiode.[12]

Results

Time-Resolved Infrared (TRIR) Experiments. It has recently been established that transient near-IR to mid-IR spectroscopy is an effective technique to measure the injection dynamics of electrons in sensitized semiconductors.[1,10] For sensitized TiO_2 samples following visible excitation, the absorbance by electrons in the TiO_2 is uniform across the entire probed region (1850−1950 cm^{-1}), and the average value as a function of time is shown in Figure 1. In Figures 1−6, the uncertainty of the intensity value is indicated by the scatter in the data points. The 1850−1950 cm^{-1} spectral region was chosen because it is free from sensitizer ground- and excited-state absorbances, namely the ν(C═O) band[10] near 1730 cm^{-1} and the ν(C≡N) band near 2100 cm^{-1}. For both **1** and **2** anchored to TiO_2 the absorption rise tracks the single-sided cross-correlation with no further increase in intensity, indicating that electron injection is complete within the excitation laser

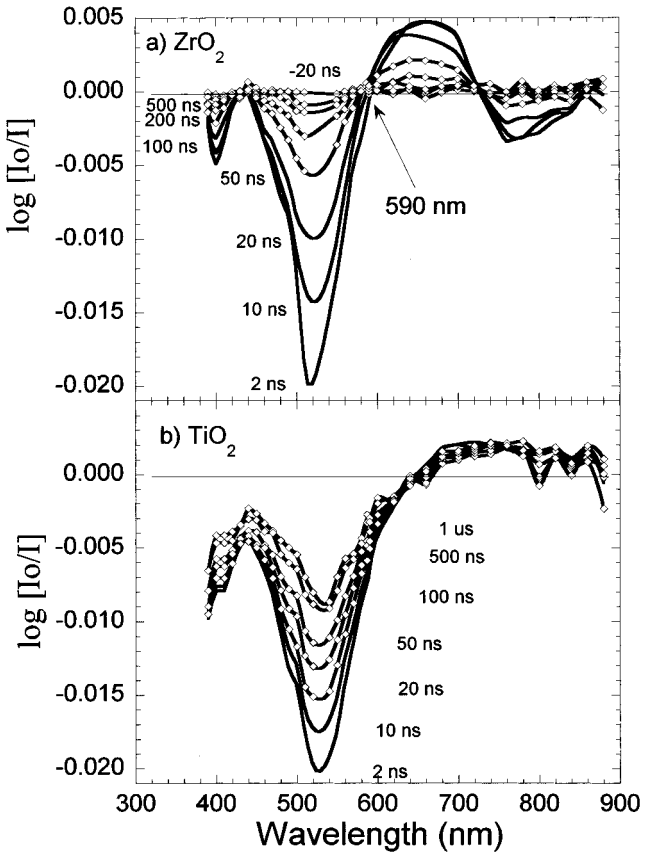

Figure 2. Transient difference spectra in the visible region of (a) ZrO_2 and (b) TiO_2 films sensitized with **1** under 532 nm, 0.1 mJ excitation. I_0 and I are the transmitted probe intensity with the 5-ns excitation pulse blocked and unblocked, respectively. Spectra are not corrected for photoluminescence of **1**/ZrO_2 observed in the 750−900 nm region.

pulse duration. This allows us to place a lower limit for k_2 of 2.9×10^{12} s^{-1}. A TRIR instrument-limited rise time for **1** on TiO_2 has previously been observed by other research groups,[1] with responses as fast as 25 fs.[1a]

The coincidence of the cross-correlation and the electron-absorbance rise time caused us to suspect that two-photon excitation of the TiO_2 could give rise to the observed signal. Substitution of nonsensitized TiO_2 for the sample revealed a small absorbance change contribution (ΔAbs = +0.005 at 8 μJ pump energy) by this effect, indicated by the arrow in Figure 1. However, the absorbance signal for **1** anchored to TiO_2 exceeds this value by a factor of 4, and displays a linear dependence on pump power in the range of 3−12 μJ. The two-photon signal for nonsensitized TiO_2 is undetectable at 3 μJ. No measurable transient absorbance was observed in the 1850−1950 cm^{-1} region for the dye molecules anchored to insulating ZrO_2, indicating that the observed transient absorbance in TiO_2 is not a thermal effect.

Transient Visible Spectroscopy. *(4,4′dcb)$_2$Ru(NCS)$_2$.* For the sensitizers anchored to transparent TiO_2 or ZrO_2 films, transient visible spectra are readily obtained. Figure 2 displays the spectra of **1** on ZrO_2 at various times following the excitation pulse. The spectra are not corrected for photoluminescence. Key features are the metal-to-ligand charge transfer (MLCT) bleach centered at 520 nm, a ligand-based absorbance band at 650 nm, and photoluminescence (PL) centered near 760 nm. These features are all typical of the excited state of **1**.[13] The spectra obtained for **1** on TiO_2 are significantly different, particularly in the near-IR. There is no measurable PL; instead a long-lived (tens of microseconds) positive absorbance persists. Contributions to this absorbance include both the ligand-to-metal charge transfer (LMCT) transition[14] of $\mathbf{1}^+$ and absorbance by electrons injected into TiO_2.[1a,15]

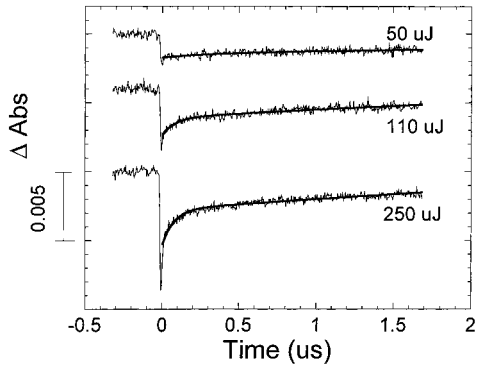

Figure 3. Oxidized dye − injected electron recombination kinetics measured at 590 nm for **1** anchored to TiO_2, as a function of excitation irradiance at 532 nm. The data are fit to the sum of a first-order and a second-order decay as described in the text.

Recombination of injected electrons with the oxidized dye (k_3) is measured by monitoring the recovery of the Ru^{II} ground-state absorbance at 590 nm. At this wavelength, there is no contribution by the excited state of **1**, as shown by the transient spectra on ZrO_2. Figure 3 displays the observed recovery kinetics as a function of excitation irradiance. As the irradiance is increased beyond 50 μJ, a fast component becomes apparent. Such behavior has been previously observed in this and similar Ru^{II} systems.[15] The recovery kinetics are modeled as the sum of a first-order and second-order decay and fit to the following equation:

$$I(t) = \alpha_a \exp(-k_a t) + \left[\frac{1}{\alpha_b} + k_b t\right]^{-1}$$

Here k_a and k_b are the first- and second-order rate constants, respectively, and α_a and α_b are the corresponding amplitudes. The observed second-order rate constant, k_b, is a function of both the extinction coefficient change ($\Delta\epsilon$) and the optical path length (l) such that k_b(observed) = k_b(actual)/($\Delta\epsilon l$). The observed rates are summarized in Table 1. The actual second-order rate can be calculated if $\Delta\epsilon$ and l are known. We have estimated $\Delta\epsilon$(590 nm) $\approx$ 1270 M^{-1} cm^{-1} from a recent report of visible absorbance spectra of **1** in aqueous solution before and after oxidation by pulse radiolysis in the presence of KBr.[14a] The optical path length can be approximated as the TiO_2 film thickness obtained from profilometry, 10 μm. The observed second-order rate of 1.6×10^8 s^{-1} for **1**/TiO_2 yields by this analysis an actual second-order rate constant of 2.0×10^8 M^{-1} s^{-1}.

Ru^{II} recovery was also measured in the presence of iodide electron donors in solution. When NaI is added in increasing amounts, recovery is faster as shown by the kinetic traces in Figure 4a. Addition of both NaI and I_2 as a redox pair allows formation of I_3^-. This has a dramatic effect on the Ru^{II} recovery in that at 0.25 mol/L NaI and 0.025 mol/L I_2, 90% of the time zero amplitude is quenched (Figure 4b). This indicates a static quenching mechanism, possibly by an adsorbed iodide species such as I_3^-. The degree of quenching at time zero is not linear in NaI and I_2 concentration, nor presumably in [I_3^-]. In fact, the quenching vs donor concentration fits the Langmuir adsorption isotherm model (Figure 4 inset), with two assumptions: (1) the degree of quenching is proportional to the number of moles of adsorbed I_3^-, and (2) the number of moles of adsorbed species is much smaller than the number of moles of solution

TABLE 1: Electron-Transfer Rates at the Sensitizer−Semiconductor Interface

system	k_{-1}[a] $\times 10^7$ s^{-1}	k_2[b] $\times 10^{12}$ s^{-1}	power[c] mJ	k_{3a}, first-order[d] $\times 10^7$ s^{-1}	k_{3b}, second-order $\times 10^8$ s^{-1}	α_a/α_b	k_4[e] $\times 10^7$ s^{-1}
1/TiO_2	4.2 ± 0.4	>2.9	0.05	0.4 ± 0.3	1.3 ± 0.4	0.15	>7.1
			0.11	1.2 ± 0.3	1.6 ± 0.2	0.48	
			0.25	1.3 ± 0.3	1.8 ± 0.1	0.62	
2/TiO_2	400 ± 36	>2.9	0.20	0.4 ± 0.3	1.6 ± 0.6	0.36	>7.1
2/SnO_2	400 ± 36	not meas'd	0.20	1.4 ± 0.2	3.2 ± 0.3	1.13	>7.1

[a] Inverse excited-state lifetime of the sensitizer dissolved in MeOH. An expanded uncertainty of 2σ is indicated throughout Table 1. [b] Electron-injection rate constant measured by time-resolved infrared absorbance. [c] Excitation energy at 532 nm. The beam diameter is ≈2 mm. [d] Observed injected electron-oxidized dye recombination rate analyzed according to the two-component model described in the text. k_{3b}(observed) = k_{3b}(actual)/($\Delta\epsilon l$). See Results section for calculation of actual second-order rates. [e] Dye reduction rate measured in a two-electrode cell with 0.5 mol/L NaI and 0.05 mol/L I_2.

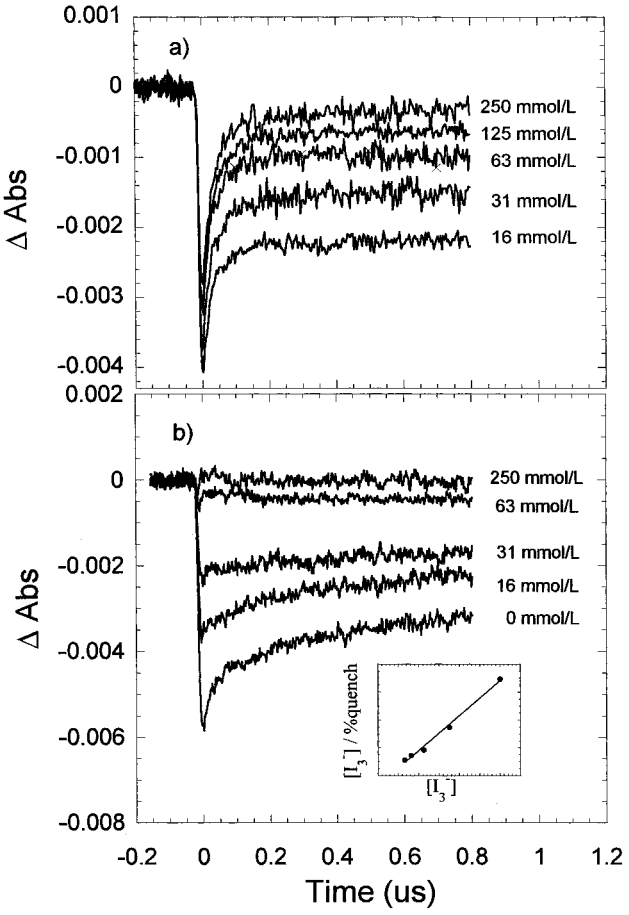

Figure 4. Quenching of oxidized **1** as a function of added (**a)** NaI or (**b)** NaI and I_2 in a 10:1 molar ratio, measured at 590 nm under 0.2 mJ, 532 nm excitation. The molarity of NaI is indicated. The inset shows a fit to the Langmuir adsorption isotherm model in terms of [I_3^-] as described in the text.

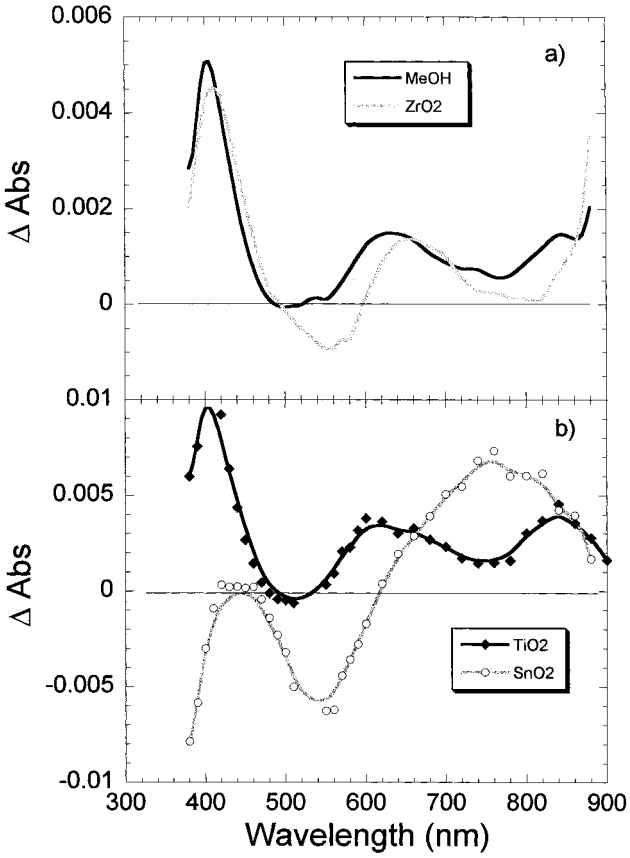

Figure 5. Transient visible absorbance spectra of **2** in MeOH or on ZrO_2 (a) and on TiO_2 or SnO_2 films (b). Spectra shown were taken at 5 ns following 532 nm, 0.1 mJ excitation for films or 570 nm excitation in MeOH.

species prior to adsorption, such that [I_3^-]$_{eq}$ ≈ [I_3^-]$_o$. These assumptions are necessary, as we are unable to quantify the concentration of adsorbed species.

(5,5′dcb)$_2$Ru(NCS)$_2$. For **2** in solution or anchored to metal oxide films, transient visible spectra are shown in Figure 5. The most prominent feature of the sensitizer in MeOH or on ZrO_2 (Figure 5a) is a positive absorbance at 400 nm, assigned to (5,5′dcb)$^-$. This absorbance somewhat overwhelms the MLCT bleach near 540 nm. A second ligand-based absorbance appears in the 600−700 nm region. The decay of all features occurs on the time scale of the instrument response (≈14 ns). This is expected, since the excited-state lifetime of **2** in MeOH is 250 ps ± 11 ps (data not shown; the expanded uncertainty [2σ] is indicated). The spectra for **2** anchored to semiconducting metal oxide films are shown in Figure 5b. For TiO_2 films sensitized with **2**, the spectrum is very similar to that of ZrO_2 except at times >20 ns, where a microsecond-lived positive absorbance persists in the near-IR. When **2** is attached to SnO_2 films, the resulting transient spectra are significantly altered. The (5,5′dcb)$^-$ absorbance at 400 nm is absent, and the MLCT bleach and near-IR absorbance are both greatly enhanced. The lifetime of these features is several microseconds.

In the absence of a strong bleach signal for **2** on TiO_2, recombination of injected electrons with the oxidized dye was measured by monitoring the decay of the electron absorbance at 820 nm. At this wavelength, the contribution from the sensitizer excited state (Figure 5a) is minimal. At excitation energies of 50 μJ, a second-order decay is observed which persists for tens of microseconds. The results are shown in Figure 6 and compared with the analogous electron decay measured for **1** on TiO_2 at 730 nm. The initial recombination kinetics measured on the picosecond time scale are also similar for the two dyes (Figure 6 inset).

The absence of a bleach for **2**/TiO_2 also required quenching by iodide species to be monitored at a different wavelength. At

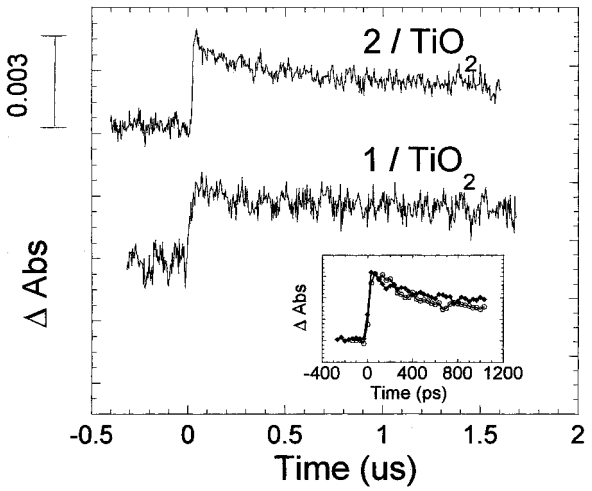

Figure 6. Oxidized dye − injected electron recombination kinetics measured at 730 nm for **1** and 820 nm for **2** anchored to TiO_2. Probe wavelengths were chosen to eliminate or minimize contributions from the sensitizer excited state. Excitation irradiance was 0.1 mJ for **1** and 0.2 mJ for **2** such that an approximately equal number of electrons were injected in each case. Kinetics measured on a picosecond time scale are shown in the inset for **1** (closed symbols) and **2** (open symbols).

437 nm, in the presence of 0.25 or 0.5 mol/L NaI, a long-lived absorbance appears, which does *not* return to baseline before the next laser pulse arrives 50 ms later. The intensity of this absorbance increases as the monitoring wavelength is shifted toward 400 nm. These features are attributed to the formation of oxidized iodide species.[16] The appearance of the absorbance is complete within the 14-ns instrument response. This implies a lower limit for the rate of I^- oxidation by $\mathbf{2}^+$ of 7×10^7 s^{-1} at 0.5 mol/L NaI concentration (1.4×10^8 mol^{-1} L s^{-1}). We note that a rate of I^- oxidation by $Ru^{III}(dcb)(bpy)_2$ anchored to SnO_2 of 1.2×10^{10} mol^{-1} L s^{-1} has recently been reported.[16] An identical instrument-response-limited absorbance in the 400−440 nm range is observed for **2** anchored to SnO_2 in electrolyte. No transient is detected upon 532 nm photolysis of the electrolyte only, with no electrode present. Table 1 summarizes the rates of electron injection, recombination, and halide oxidation for the systems under study.

Photoelectrochemistry. Steady-state photocurrents were measured for sensitized metal oxide electrodes in a two-electrode arrangement with 0.5 mol/L NaI and 0.05 mol/L I_2 electrolyte in propylene carbonate. Incident photon-to-current efficiencies (IPCEs) are calculated using the following equation:

$$\mathrm{IPCE} = \frac{(1240\ \mathrm{eV{\cdot}nm})(\text{photocurrent density } \mu\mathrm{A/cm^2})}{(\text{wavelength nm})(\text{irradiance } \mu\mathrm{W/cm^2})}$$

Dividing the IPCE by the fraction of incident photons absorbed at each wavelength (termed light harvesting efficiency, see Discussion section) gives the absorbed photon-to-current efficiency (APCE), shown in Figure 7 for **1** and **2** on TiO_2 or SnO_2. The indicated uncertainty reflects the combined expanded uncertainty of the absorbance, photocurrent, wavelength, and detector responsivity. The latter dominates at short wavelength. The APCE for **2** improves significantly when the sensitizer is bound to SnO_2, and a value of ≈40% independent of wavelength from 350 to 760 nm is achieved. Photocurrent measurements were performed primarily with illumination through the substrate side of the sensitized metal oxide electrodes. However, APCE spectra measured with "backside illumination" through the Pt

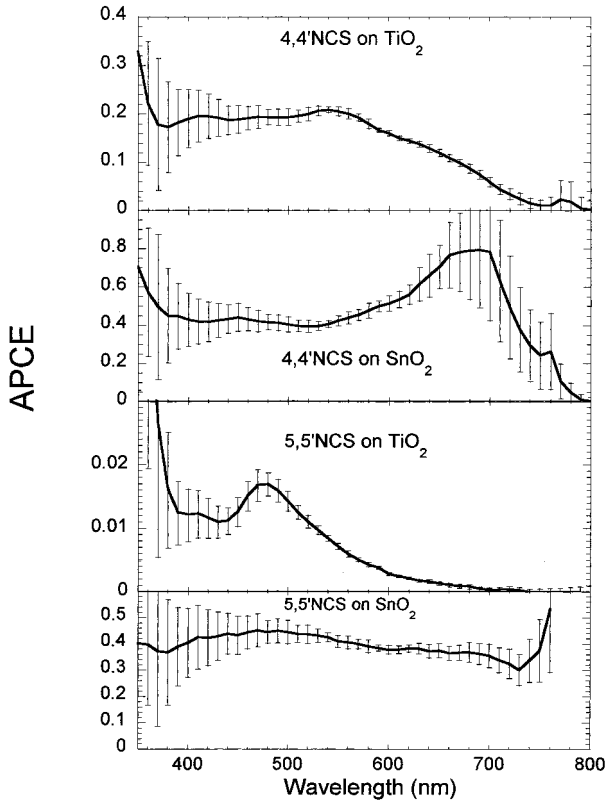

Figure 7. Photon-to-current conversion efficiency for sensitized metal oxide electrodes in a two-electrode solar cell with NaI/I_2 electrolyte. Efficiencies are corrected for the fraction of incident photons absorbed by the sensitizer at each wavelength, see text for details.

counter electrode revealed no significant difference for wavelengths greater than 500 nm.

Discussion

As shown in the energy level diagram (Scheme 1), the ground-state $Ru^{III/II}$ oxidation potentials for **1** and **2** measured in solution are identical within experimental error.[3] Attempts using cyclic voltammetry to estimate the $Ru^{III/II}$ potential for the compounds anchored to TiO_2 substrates have been unsuccessful. However, any shift upon surface attachment is expected to be similar for these two closely related sensitizers. If the reduction potentials of surface-anchored $\mathbf{1}^+$ and $\mathbf{2}^+$ are in fact similar, one would expect similar rates of recombination (k_3) and halide oxidation (k_4). We have used a model which incorporates both first-order and second-order recombination processes to describe the observed recombination kinetics. The justification of this model is as follows:

Visible and electron paramagnetic resonance (EPR) spectroscopy of electrochemically reduced TiO_2 films suggests that a significant number of injected electrons reside in Ti^{IV} sites as Ti^{III}.[17] For some photoinjected electrons, the Ti^{III} sites may be those directly bound to sensitizer molecules. In this case the charge-separated state and recombination reaction are depicted as the following:

$$Ti^{III}\text{-}|\text{-}Ru^{III} \xrightarrow{k_3} Ti^{IV}\text{-}|\text{-}Ru^{II}$$

No diffusion of the reactants is required, and the charge recombination should follow first-order kinetics. The fast initial exponential component of the decay in Figure 3 is attributed to this "geminate" recombination. A second possibility is that the electron diffuses from a remote Ti^{III} site before recombination

occurs. This idea is consistent with the electron-hopping mechanisms proposed for the conduction mechanism in colloidal anatase TiO_2 films.[18] Under these conditions the recombination would resemble a bimolecular process where the electron must diffuse toward the oxidized sensitizer:

$$e^- (TiO_2\,\text{bulk}) + |\text{-}Ru^{III} \xrightarrow{k_3} |\text{-}Ru^{II}$$

For this process, second-order kinetics would be expected. The best evidence for a second-order kinetic model comes from second-order equal-concentration (of Ru^{III} and electrons in TiO_2) kinetic rate constants that are independent of the Ru^{III} and $TiO_2(e^-)$ concentration. In previous work we have shown that when the initial concentration of Ru^{III} and $TiO_2(e^-)$ was varied by a factor of greater than 20 by changing the excitation irradiance or ionic strength, the abstracted second-order equal-concentration kinetic rate constant was unchanged.[15b] A similar result is obtained in this study: values of k_{3b} for **1**/TiO_2 in Table 1 are identical within experimental error for excitation energies of 50−250 μJ. This is typically not true for the commonly used stretched exponential models (i.e., Kohlrausch,[19a] Williams and Watts[19b]).

The kinetics shown in Figure 6 and the recovered rates listed in Table 1 indicate similar recombination kinetics (k_3) for **1** and **2** anchored to TiO_2. It is concluded that both $\mathbf{1}^+$ and $\mathbf{2}^+$ can effectively oxidize the iodide donors, primarily I^- and I_3^-, within the several-microsecond window of recombination. Quenching of the oxidized dye for **1**/TiO_2 in the presence of both I^- and I_2 (Figure 4b and inset) indicates that dye reduction in working solar cells involves a mechanism which is static during the 14-ns resolution of our instrument.

We now turn to the competition between electron injection (k_2) and excited-state decay (k_{-1}). The TRIR results in Figure 1 indicate that it is possible to lower the sensitizer excited-state potential[4] by 200 mV and still have electron injection occur faster than 350 fs . Two possible explanations for this behavior are (1) the acceptors in the TiO_2 form a broad continuous energy band, overlapping well with both sensitizer excited states, and (2) ultrafast electron transfer at these interfaces differs completely from the Marcus−Gerischer "weak electronic interaction" electron transfer and does not involve redistribution of vibrational excitation energy. In this case electron injection precedes excited-state vibrational relaxation. The latter concept has been suggested by Willig and co-workers, who observed <25 fs electron transfer from **1** to TiO_2 using an 1100-nm probe.[1a] The smaller electron-absorbance signal observed in the case of **2** (0.01 vs 0.02 for **1**, Figure 1) suggests an ≈50% lower electron-injection yield. From a kinetic argument, this is surprising. Even if the injection rate is as slow as 2.9×10^{12} s^{-1}, it is still 3 orders of magnitude faster than the excited-state decay of **2**, which is 4.0×10^9 s^{-1} measured in MeOH (Table 1).

A reduced injection yield for **2**/TiO_2 is also indicated by the transient visible spectroscopy. Spectra for **1** in Figure 2 indicate significant absorbance changes when the sensitizer is bound to TiO_2 vs ZrO_2, attributed to **1** in the oxidized state and injected electrons in TiO_2. For **2,** the spectra on TiO_2 and ZrO_2, as well as in solution, are similar (Figure 5). This suggests that the majority of dye molecules are in the excited state, rather than in the oxidized form. However, when **2** is anchored to SnO_2, the excited-state ligand absorbance at 400 nm disappears, an MLCT bleach is present, and near-IR absorbance by injected electrons is evident. Thus, it is possible to achieve efficient injection from **2** by using an alternative semiconductor with lower energy-acceptor states. It is unclear at this point whether the acceptor states fall within the SnO_2 conduction band, are Sn^{IV} traps, are surface states, or a combination of all these possibilities.

If recombination (k_3) is not a significant loss mechanism in the working solar cell, and the dye-absorbance characteristics are known, then the electron-injection yield can be estimated through careful photocurrent measurements. The incident photon-to-current efficiency (IPCE) is a product of three terms:

$$\text{IPCE} = \text{LHE}\,(\phi_{\text{inj}})(\eta)$$

Here, LHE is the light harvesting efficiency or absorptance, defined as $\text{LHE} = 1-10^{-A}$ where A is the sample absorbance; ϕ_{inj} is the quantum yield for electron injection; and η is the efficiency of transporting injected electrons to the external circuit. It is well known that LHE is wavelength dependent, being related to the sensitizer absorbance spectra. The wavelength dependences of ϕ_{inj} and η are less certain. Dividing the IPCE by the LHE gives the absorbed photon-to-current efficiency (APCE), shown in Figure 7 for **1** and **2** anchored to TiO_2 or SnO_2:

$$\text{APCE} = \frac{\text{IPCE}}{\text{LHE}} = (\phi_{\text{inj}})(\eta)$$

Thus, the APCE should reflect the wavelength dependence of ϕ_{inj} and η. For **1** on TiO_2 the APCE clearly drops off in the 600−700 nm range. When the same sensitizer is anchored to SnO_2, the APCE in the 400−600 nm range improves to 40% (vs 20% on TiO_2) and actually *increases* for wavelengths of 600−700 nm. For **2**/TiO_2 the decrease in APCE at low energy is even more dramatic and begins at 500 nm. For **2**/SnO_2 the APCE response is uniform within experimental error, indicating efficient injection at all energies. With the exception of **2**/SnO_2, the shapes of the APCE spectra indicate a wavelength dependence for ϕ_{inj} or η or possibly both. Transport efficiency (η) could be wavelength dependent if electrons injected at a greater distance from the conductive substrate (i.e., low-energy photons with illumination through the indium-doped tin oxide substrate) experienced greater loss during migration through the film. However, when the cell is illuminated from the backside[18a,b] (through the Pt counter electrode) the APCE spectra are unchanged at $\lambda > 500$ nm. Thus, we conclude that the APCE spectra reflect the wavelength dependence of ϕ_{inj}. A simple explanation for the wavelength dependence of ϕ_{inj} is that the excited state of **2** is not sufficiently energetic to inject into TiO_2. However, the lower energy acceptor states of SnO_2 enable efficient injection from **2** at all visible wavelengths.

The reason for the reproducible *increase* in injection efficiency for **1**/SnO_2 between 600 and 700 nm is not obvious. Perhaps a low-energy surface state exists in SnO_2 which has enhanced orbital overlap with the excited state of **1** at this energy.

Moser and Grätzel[20] have shown that for **1**/TiO_2, ϕ_{inj} is wavelength independent in the range 450−680 nm but does decrease at $\lambda > 550$ nm for **1**/Nb_2O_5 where the conduction band lies 0.2−0.3 eV higher in energy vs. TiO_2. It is possible that our film preparation and other experimental conditions differ in such a way as to yield TiO_2 materials with acceptor states which are higher in energy than those studied by Moser. This could explain our observed wavelength dependence for **1**/TiO_2.

The reproducible order of magnitude decrease in APCE for **2**/TiO_2 relative to **1**/TiO_2 is surprising. Our previous work comparing the efficiency of these two sensitizers on opaque

TiO_2 films prepared from Degussa P25 TiO_2 particles revealed only a factor of 2 difference in IPCE.[3] In an effort to resolve this inconsistency we have successfully reproduced the relative efficiencies of **1** and **2** on Degussa TiO_2. If the transparent TiO_2 films used in this study possess higher energy-acceptor states as suggested above, overlap with the excited state of **2** could be insufficient for effective electron injection. The discrepancy between the injection yields inferred from Figures 1b and 7 for compound **2** on TiO_2 is also remarkable. We can only surmise that the inconsistency results from the different experimental conditions used in the two cases. The photocurrent experiment (Figure 7) uses steady-state excitation of the complete solar cell with NaI/I_2 electrolyte. The TRIR experiment uses a 200-fs pulse excitation of the photoanode only, with no electrolyte present. We are, unfortunately, not yet able to determine which, if any, of these differences accounts for the discrepancy.

The efficient sensitization of SnO_2 with **2** at all wavelengths of the MLCT absorbance band is encouraging, as sensitizer **2** holds particular promise for efficient solar cells. When the MLCT absorbance band is integrated over the Air Mass 1.5 solar spectrum,[21] an overall solar light harvesting efficiency of 27% is achieved. If a reasonable 80% of absorbed photons can be converted to electrons, as in the case of **1** and other sensitizers[22] anchored to opaque TiO_2, an impressive 22% solar efficiency would result. We are currently attempting to prepare high surface area SnO_2 films with a thickness of several micrometers in hopes of approaching this value.

Conclusions

A detailed set of time-resolved infrared, UV−vis, and photocurrent measurements for $(4,4'dcb)_2Ru(NCS)_2$ and $(5,5'dcb)_2Ru(NCS)_2$ adsorbed on ZrO_2, TiO_2, and SnO_2 nanocrystalline-film substrates have been performed. These studies were conducted with the aim of identifying inherent electron-transfer processes responsible for an observed difference in photon-to-electron conversion efficiencies for the above sensitizers in photoconductive TiO_2 solar cells. Ultrafast injection rates for both dyes on TiO_2 suggest that wavelength-dependent cell efficiencies are probably governed by coupling of the donor excited-state levels with appropriate accepting levels of the substrate. In addition, measurements were conducted to monitor transient UV−vis spectra and kinetics to identify the competition between back electron transfer and oxidized dye quenching by added iodine electron donors (e.g., I^-, I_3^-) as a function of iodine ion concentration. Both sensitizers can effectively oxidize the halide donors on the time scale of back electron transfer.

We have also shown that absorbance-corrected photocurrent measurements provide useful determinations of electron-injection and transport yields. When donor/acceptor overlap is less than ideal, decreased electron-injection yields are observed. The effect is most dramatic at long excitation wavelengths. Most importantly, it was demonstrated that efficient electron injection over the 350−800 nm wavelength range can be achieved with the red-shifted sensitizer $(5,5'dcb)_2Ru(NCS)_2$. This was accomplished by employing SnO_2 as an alternative to the semiconductor TiO_2. Apparently, tin oxide has energy-acceptor states that overlap well with sensitizers having low-energy donating levels. Even under these conditions, the injected electron-to-oxidized sensitizer recombination rate is not significantly affected. On the basis of our observations, solar cells constructed with either dye on transparent SnO_2 substrates are expected to function with extremely high photon-to-electron conversion efficiencies.

References and Notes

(1) (a) Hannappel, T.; Burfeindt, B.; Storck, W.; Willig, F. *J. Phys. Chem. B* **1997**, *101*, 6799. (b) Heimer, T. A.; Heilweil, E. J. *Ultrafast XI*; Elsaesser, T., Fujimoto, J. G., Wiersma, D. A., Zirth, W., Eds.; Springer-Verlag: New York,1998; p 505. (c) Ellingson, R. J.; Asbury, J. B.; Ferrere, S.; Ghosh, H. N.; Sprague, J. R.; Lian, T.; Nozik, A. *J. Phys. Chem. B* **1998**, *102*, 6455.

(2) Heimer, T. A.; Bignozzi, C. A.; Meyer, G. J. *J. Phys. Chem.* **1993**, *97*, 11987.

(3) Argazzi, R.; Bignozzi, C. A.; Heimer, T. A.; Castellano, F. N.; Meyer, G. J. *Inorg. Chem.* **1994**, *33*, 5741.

(4) Ground-state RuIII/II potentials were reported in ref 3. The E_{00} energy of **1** (1.95 eV) is taken from the 5% level of the emission spectra in ref 20a. In the absence of emission from the fully protonated form of **2**, we have estimated the E_{00} energy from the low-energy absorbance onset. The excited-state reduction potential D^* is calculated as $D^* = E(Ru^{III/II}) - E_{00}$. This analysis yields $D^* = -1.0$ and -0.8 V vs SCE for **1** and **2,** respectively.

(5) (a) Gerischer, H. *Pure Appl. Chem.* **1980**, *52*, 2649. (b) Fessenden, R. W.; Kamat, P. V. *J. Phys. Chem.* **1995**, *99*, 12902.

(6) O'Regan, B.; Moser, J.; Anderson, M.; Grätzel, M. *J. Phys. Chem.* **1990**, *94*, 8720.

(7) Heimer, T. A.; D'Arcangelis, S. T.; Farzad, F.; Stipkala, J. M.; Meyer, G. J. *Inorg. Chem.* **1996**, *35*, 5319.

(8) Lemon, B. I.; Hupp, J. T. *J. Phys. Chem. B* **1997**, *101*, 2426.

(9) Disclaimer: Certain commercial equipment, instruments, or materials are identified in this paper in order to adequately specify the experimental procedure. In no case does such identification imply recommendation or endorsement by the National Institute of Standards and Technology, nor does it imply that the materials or equipment identified are necessarily the best available for the purpose.

(10) Heimer, T. A.; Heilweil, E. J. *J. Phys. Chem. B* **1997**, *101*, 10990.

(11) (a) Heilweil, E. J.; Cavanagh, R. R.; Stephenson, J. C. *Chem. Phys. Lett.* **1987**, *134*, 181. (b) Dougherty, T. P.; Heilweil, E. J. *Opt. Lett.* **1994**, *19*, 129.

(12) The Si photodiode was calibrated following the procedure in Larason, T. C.; Bruce, S. S.; Parr, A. C. *Spectroradiometric Detector Measurements*; NIST special publication 250-41; U.S. Department of Commerce, National Institute of Standards and Technology, U.S. Government Printing Office: Washington, DC, 1998.

(13) Published spectra vary at wavelengths greater than 700 nm, due to differences in photoluminescence collection efficiency. See for example: Tachibana, Y.; Moser, J. E.; Grätzel, M.; Klug, D. R.; Durrant, J. R. *J. Phys. Chem.* **1996**, *100*, 20056.

(14) (a) Das, S.; Kamat, P. V. *J. Phys. Chem. B* **1998**, *102*, 8954. (b) Moser, J. E.; Noukakis, D.; Bach, U.; Tachibana, Y.; Klug, D. R.; Durrant, J. R.; Humphry-Baker, R.; and Grätzel, M.. *J. Phys. Chem. B* **1998**, *102*, 3649.

(15) (a) Haque, S. A.; Tachibana, Y.; Klug, D. R.; Durrant, J. R. *J. Phys. Chem. B* **1998**, *102*, 1745. (b) Kelly, C. A.; Farzad, F.; Thompson, D. W.; Stipkala, J. M.; Meyer, G. J. *Langmuir* **1999**, *15*, 7047. (c) Heimer, T. A. Electron Transfer Kinetics in Molecular Photovoltaic Devices. Ph.D. Dissertation, Johns Hopkins University, Baltimore, MD, July 1996.

(16) Nasi, C.; Hotchandani, S.; Kamat, P. V. *J. Phys. Chem. B* **1998**, *102*, 4944.

(17) (a) Cao, F.; Oskam, G.; Searson, P. C.; Stipkala, J. M.; Heimer, T. A.; Farzad, F.; Meyer, G. J. *J. Phys. Chem.* **1995**, *99*, 11974. (b) Rothenberger, G.; Fitzmaurice, D.; Grätzel, M. *J. Phys. Chem.* **1992**, *96*, 5983.

(18) (a) Södergren, S.; Hagfeldt, A.; Olsson, J.; Lidquist, S.-E. *J. Phys. Chem.* **1994**, *98*, 5552. (b) Rensmo, H.; Linstrom, H.; Södergren, S.; Lindquist, S.-E. In *Nanostructured Materials in Electrochemistry*; Searson, P. C., Meyer, G. J., Eds.; The Electrochemical Society: Pennington, New Jersey, 1995; Vol. 95−8, p 67. (c) Oskam, G.; Cao, F.; Searson, P. C. In *Nanostructured Materials in Electrochemistry*; Searson, P. C., Meyer, G. J., Eds.; The Electrochemical Society: Pennington, New Jersey, 1995; Vol. 95−8, p 98.

(19) (a) Kohlrausch, R. *Justus Liebigs Ann. Chem.* **1847**, *5*, 430. (b) Williams, G.; Watts, D. C. *Trans. Faraday Soc.* **1971**, *66*, 80.

(20) Moser, J. E.; Grätzel, M. *Chimia* **1998**, *52*, 160.

(21) *Standard Tables for Terrestrial Solar Spectral Irradiance at Air Mass 1.5 for a 37 Degree Tilted Surface*; E892-87; ASTM: Philadelphia, PA, 1987.

(22) (a) Nazeeruddin, M. K.; Kay, A.; Rodicio, I.; Humphry-Baker, R.; Müller, E.; Liska, P.; Vlachopoulos, N.; Grätzel, M. *J. Am. Chem. Soc.* **1993**, *115*, 6382. (b) Nazeeruddin, M. K.; Liska, P.; Moser, J.; Vlachopoulos, N.; Grätzel, M. *Helv. Chim. Acta* **1990**, *73*, 1788.